X-ray Absorption Spectromicroscopy Studies for the Development of Lithography with a Monomolecular Resist

M. Zharnikov,*,† A. Shaporenko,† A. Paul,† A. Gölzhäuser,†,‡ and A. Scholl§

Angewandte Physikalische Chemie, Universität Heidelberg, Im Neuenheimer Feld 253, 69120 Heidelberg, Germany, and Advanced Light Source, Ernest Orlando Lawrence Berkeley National Laboratory, Berkeley, California 94720

Received: October 7, 2004; In Final Form: January 20, 2005

Soft X-ray absorption microscopy was applied to image and characterize molecular patterns produced by electron irradiation of aliphatic and aromatic thiol-derived self-assembled monolayers (SAMs) on Au substrates. The measurements were performed at all relevant absorption edges. The fabricated patterns could be clearly imaged with a lateral resolution better than 150 nm, which, for example, allowed us to distinguish a fine structure of 1 μm features. The X-ray absorption microspot spectra derived from different areas of the SAM patterns provided specific chemical information on pristine and irradiated areas and unexpected features in these patterns. The quality of the microspot spectra is comparable with that of the analogous X-ray absorption spectra acquired with standard equipment from homogeneous SAMs. In particular, a chemical transformation of the functional tail groups within the irradiated areas of the patterned aromatic SAMs could be directly monitored.

1. Introduction

The increasing miniaturization of integrated devices and new areas of biology and medicine demand the development of new methods for the fabrication of micro- and nanostructures. One of the perspective approaches applies X-ray and electron-beam patterning of a new kind of lithographic resist—self-assembled monolayers (SAMs).[1−15] These are well-ordered and densely packed two-dimensional (2D) ensembles of amphiphilic molecules, chemisorbed on a suitable substrate.[16,17] The relevant molecules consist of three essential parts, namely, a headgroup that binds strongly to the substrate, a tailgroup that constitutes the outer surface of the film, and a rodlike spacer that connects head and tail groups. In the case of X-ray or electron-beam lithography, the patterning of the SAMs occurs either with the help of a mask in so-called proximity printing geometry or by scanning a focused beam over the film. Due to the monolayer thickness and molecular character of the SAM resist, the fabrication of structures down to the scale of several nanometers is in principle possible (see, for example, ref 18). An additional advantage of SAM resists is the dependence of the changes induced by ionizing radiation on the character of the SAM constituent. Whereas such an irradiation results in damage and disordering of aliphatic SAMs (a positive resist),[19−24] a quasi-polymerization with an only partial disordering occurs in the films with the aromatic spacer (a negative resist).[25−27] What is even more important, the resistance of the aromatic SAMs toward ionizing radiation makes possible a selective chemical modification of specific tailgroups, enabling the fabrication of chemical lithographic patterns and templates.[26,28,29] The fabricated lithographic patterns can be subsequently used for laterally selective attachment of other moieties or biological macromolecules such as cells, proteins, or specific receptors.[26]

The progress achieved in the field of SAM-based lithography was only possible on the basis of detailed spectroscopic characterization of the irradiation-induced changes in SAMs.[12] Such characterization was mostly performed on homogeneously irradiated samples,[12,19−26] whereas the lithographic patterns were preferentially imaged by atomic force microscopy or scanning electron microscopy (see, for example, ref 29). Whereas such imaging provided useful information about the topographic profile of the lithographic patterns, the more important chemical information was not available. This information can only be obtained by a spectromicroscopic approach. So far, only X-ray photoelectron spectromicroscopy (XPM) with a zone-plate-focused X-ray beam has been tested.[15,30,31] However, whereas this technique succeeded in chemical imaging of SAM-based lithographic patterns, a lateral resolution was rather limited (0.5 μm)[15] and there were significant problems with X-ray beam damage and a comparably large inelastic background. In particular, it was therefore not possible to image and monitor the irradiation-induced chemical modification of the functional tailgroups in aromatic SAMs.[31]

In this study we apply an alternative spectromicroscopic approach, namely, X-ray absorption spectromicroscopy (XAM) for chemical imaging and microspectroscopic characterization of SAM-based lithographic patterns. Note that in XAM or closely related X-ray absorption near-edge fine structure (NEXAFS) spectroscopy experiments, core-level electrons (e.g., C 1s for a C K-edge spectrum) are excited into nonoccupied molecular orbitals, which are characteristic for specific bonds, functional groups, or molecules. The photon energy positions of the respective absorption resonances give then a clear signature of these entities. The lateral distribution of these entities or their specific chemical states is then provided by emission images acquired at the respective photon energies.

* Corresponding author: e-mail Michael.Zharnikov@urz.uni-heidelberg.de.

† Universität Heidelberg.

‡ Present address: Physik Supramolekularer Systeme, Universität Bielefeld, Universitätsstr. 25, 33615 Bielefeld, Germany.

§ Ernest Orlando Lawrence Berkeley National Laboratory.

10.1021/jp040649g CCC: $30.25
Published on Web 02/26/2005

In addition to the spectromicroscopic data, we present some results obtained by conventional spectroscopic techniques. These results are considered as a reference and complementary information to the XAM data.

In the following section we describe the experimental procedures and techniques. The results are presented and briefly discussed in section 3. An extended analysis of the data is given in section 4, followed by a summary in section 5.

2. Experimental Section

The substrates were prepared by deposition of 100−300 nm of gold on titanium-primed polished single-crystal Si(100) wafers. These films predominantly exhibit a (111) orientation[32] and are a standard support for SAMs. The SAMs were formed by immersion of the substrates in 1 mM solutions of *n*-alkanethiol [AT; $CH_3(CH_2)_{17}SH$, octadecanethiol] or 4-nitro-1,1′-biphenyl-4-thiol [NBPT; $O_2N(C_6H_4)_2SH$] in ethanol or dichloromethane for 24 h with subsequent rinsing and drying. AT was purchased from Fluka; details of the NBPT synthesis can be found elsewhere.[26]

The patterning of the SAMs was performed by electrons with an energy of 300 eV in the proximity printing geometry. As masks, we used standard quadratic meshes with a 7.5−15 μm periodicity (Plano) and carbon Quantifoil membranes with 1.0−1.2 μm circular hole arrays, arranged in squares (Plano). The doses were 10 and 30 mC/cm^2 for AT/Au and NBPT/Au, respectively. The patterning was carried out in ultrahigh vacuum (UHV) at room temperature. The fabricated patterns were put into argon-filled glass containers and kept there for several days until the characterization that was performed in UHV. There was, however, exposure to ambient atmosphere during the sample handling between the preparation, storage, and characterization.

The spectromicroscopic characterization of the SAM-based patterns was performed at a microscopy branch (7.3.1.1) of the beamline 7.3.1 at the Advanced Light Source in Berkeley, CA. This branch operates over the photon energy range from 175 to 1500 eV with a spectral resolving power between 1000 and 2000. It is equipped with an X-ray photoelectron emission microscope (X-PEEM), which operates in the total electron yield (TEY) acquisition mode and provides a spatial resolution of typically 50−100 nm for elemental contrast imaging.

Stacks of successive NEXAFS images over the photon energy ranges containing the relevant C, N, and O K-edges were acquired in the grazing incidence geometry. Special care was taken to avoid X-ray damage during the image acquisition. The necessary steps included the selection of a new area for every new image stack, optimizing the beamline slits, putting a Ti foil into the light track (in some cases), and using an aperture to restrict the illuminated area.

By integrating over selected areas of the collected images, the C, N, and O K-edge NEXAFS microspot spectra were derived for both the pristine and irradiated regions of the SAM patterns. A conventional normalization procedure was applied, including normalizing the raw spectra to the monochromator transmission, subtracting the preedge signal, and scaling the edge jump to get an intensity of unity at 35−40 eV above the absorption edge.[33]

As a reference for the spectromicroscopy data, standard NEXAFS measurements on pristine and homogeneously irradiated AT and NBPT SAMs were carried out. The irradiation was performed under the same conditions as the patterning but without a mask. The NEXAFS experiments were carried out at the HE-SGM beamline of the synchrotron storage ring BESSY II in Berlin, Germany. The spectra were acquired at the C, N, and O K-edges in the partial electron yield (PEY) mode with a retarding voltage of −150 V. The incidence angle of the X-ray beam was 55°. The raw NEXAFS spectra were normalized to the incident photon flux by division through a spectrum of a clean, freshly sputtered gold sample. The conventional normalization procedure was applied (see above). The energy scale was referenced to the pronounced π_1* resonance of highly oriented pyrolytic graphite (HOPG) at 285.38 eV.[34]

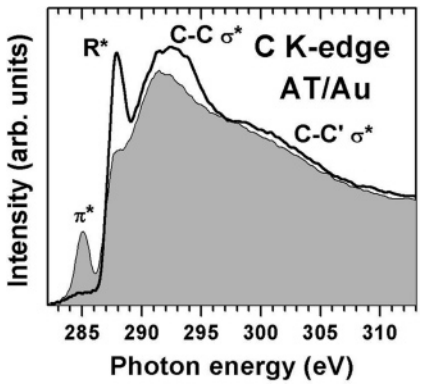

Figure 1. Large-area normalized C K-edge NEXAFS spectra of pristine (thick line) and homogeneously irradiated (shadowed) AT/Au.

To underline the chemical modification of the NBPT film by ionizing radiation, we performed high-resolution X-ray photoelectron spectroscopy (HRXPS) measurements on the respective sample in the course of X-ray irradiation. Note that the respective results are directly relevant for the case of e-beam lithography with a SAM resist, since the major impact of X-ray irradiation is provided by photoelectrons and inelastic secondary electrons.[12,24,35] The HRXPS experiments were carried out at the undulator beamline I311 at the MAX II storage ring of the MAX-lab synchrotron radiation facility in Lund, Sweden. The irradiation was provided by the beamline itself. The opening of the beamline slits was periodically varied for either the irradiation (a wide opening) or spectra acquisition (a small opening). The HRXPS spectra were acquired in normal emission geometry at photon energies of 200−500 eV. The binding energy scale was referenced to the Au $4f_{7/2}$ emission of AT-covered Au substrate at 83.95 eV.[36,37] The energy resolution was about 50 meV, which is noticeably smaller than the full widths at half-maximum (fwhm) of the photoemission peaks addressed in this study. Thus, these fwhms are representative for the natural width of the respective lines.

3. Results

3.1. HRXPS and NEXAFS Spectroscopy. Normalized C K-edge NEXAFS spectra of pristine (thick line) and homogeneously irradiated (shadowed) AT/Au are shown in Figure 1. The spectrum of the pristine film is dominated by a characteristic R* resonance at ≈287.7 eV, which is accompanied by broader C−C σ* and C−C′ σ* resonances at ≈293.4 and ≈301.6 eV, respectively. All above-mentioned resonances can be considered as fingerprints of an intact aliphatic chain in all-trans conformation.[38−42] In accordance with the previous data,[12,20,21,23] the electron bombardment results in decreasing intensity of the NEXAFS resonances and leads to the appearance of a new resonance at ≈285.1 eV, characteristic for C═C double bonds (π* resonance). These changes are caused by the orientational and conformational disordering, desorption of hydrogen- and carbon-containing fragments, and the appearance of C═C double bonds in the irradiated films.[12]

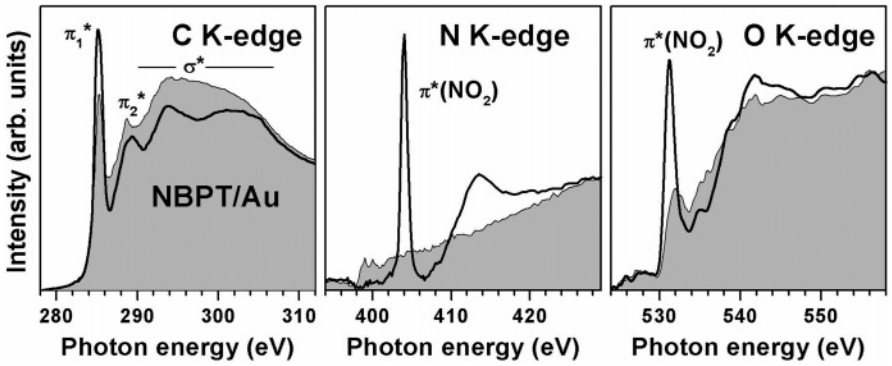

Figure 2. Large-area normalized C, N, and O K-edge NEXAFS spectra of pristine (thick line) and homogeneously irradiated (shadowed) NBPT/Au.

Large-area C, N, and O K-edge NEXAFS spectra of pristine (thick line) and homogeneously irradiated (shadowed) NBPT/Au are presented in Figure 2. The C K-edge spectrum of the pristine film is dominated by a characteristic π_1* resonance of the phenyl ring at ≈285.1 eV, accompanied by several less intense π* resonances and broad σ* features at higher photon energy.[25,42] The N and O K-edge spectra are dominated by a sharp π* resonance, at 404.0 and 531.4 eV, respectively, which can be unequivocally assigned to the nitro (-NO_2) tailgroup.[43] There are also some σ*-like features.

The electron bombardment results in decreasing intensity of the characteristic π* and σ* resonances in the C K-edge spectrum[25,42] and a drastic reduction in the intensity of the π(-N*O_2) and π(-NO*$_2$) resonances in the N and O K-edge spectra. The change of the C K-edge spectra is related to a partial dehydrogenation of the biphenyl moieties, occurring upon the irradiation-induced scission of the C−H bonds.[25] This process is followed by an extended cross-linking of the residual aromatic backbones. We assume that no disintegration of the biphenyl moieties beyond their dehydrogenation occurs, so that these are mainly C−C bonds, which are responsible for the cross-linking.[18,25] In fact, the general shape of both C K-edge NEXAFS and C 1s HRXPS (not shown) spectra remains almost the same upon irradiation and there is only a small thickness reduction. In addition, an extended disintegration of the aromatic backbones will result in the appearance of C═C bonds, which will subsequently lead to the development of the $\pi^*_{C=C}$ resonance at almost the same photon energy as the "original" π_1* peak of phenyl.[33] No significant intensity reduction at this photon energy, as it is observed in Figure 2, can then be expected upon irradiation.

The change of the N and O K-edge spectra is associated with an irradiation-induced modification of the nitro tailgroups. The strong intensity reduction of the characteristic π* resonances suggests that almost all nitro tailgroups have undergone this modification at a given dosage. The only new characteristic features observed in the spectra of the irradiated NBPT/Au are two low-intensity resonances around 400 eV in the N K-edge spectrum. Even though weak, these resonances can be associated with a nonprotonated amino group, for which a resonance structure around 398−400 eV can be expected.[44] A small intensity of the resonances can be related to the chemical state inhomogeneity of the emerging amino tailgroups. Literature data suggest a strong dependence of the observed resonance structure at the N K-edge on the state of the amino group, that is, protonated, nonprotonated, or a negative ion.[44−46]

The conclusion on the irradiation-induced nitro−amino transformation can be supported by XPS[26] or HRXPS data. In Figure 3, large-area N 1s HRXPS spectra of NBPT/Au succes-

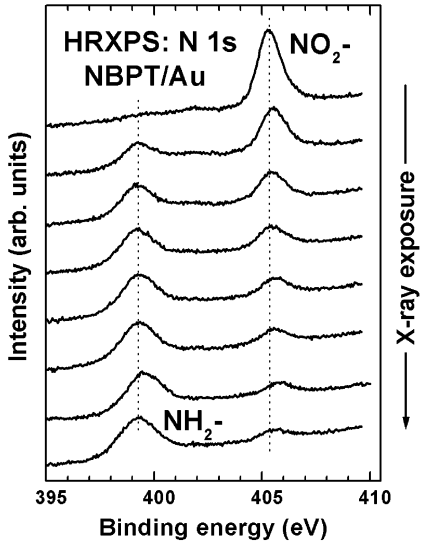

Figure 3. Large-area N 1s HRXPS spectra of NBPT/Au in the course of homogeneous X-ray irradiation. The emissions related to the amino and nitro tailgroups are marked.

sively collected in the course of homogeneous X-ray irradiation are presented. The spectrum of the pristine film (on top) exhibited a single emission assigned to the intact nitro tailgroup of NBPT.[26] In the course of the irradiation, the intensity of this feature continuously decreased, whereas a new emission at 399.3 eV appeared and continuously grew. The latter emission can be assigned to a nonprotonated amino (-NH_2) group,[44,47] which supports the above conclusion regarding the irradiation-induced transformation of the nitro tailgroup into the amino moiety. It is also in full agreement with previous results.[12,26] Interestingly, fwhms of the emissions related to the nitro and amino groups in NBPT films, 1.32 and 2.15 eV, respectively, are noticeably larger than the corresponding values for other SAMs, for example, 0.78 eV for SAMs of nitrile-functionalized ATs.[48] This suggests a chemical state inhomogeneity for these groups, which is especially pronounced in the case of amino moieties in the irradiated NBPT films, in full agreement with the conclusion derived on the basis of the N K-edge NEXAFS spectra. Note that amino groups remain in the same place as the nitro groups, that is, in the position as a tailgroup, after the nitro−amino transformation. In particular, the presence of an amino group in the tailgroup position was shown by their reaction with different anhydrides.[26,29]

3.2. NEXAFS Spectromicroscopy and Microspectroscopy. The noticeable changes in the NEXAFS spectra upon X-ray or electron irradiation were a good starting point for the NEXAFS spectromicroscopy experiments. In fact, both AT and NBPT

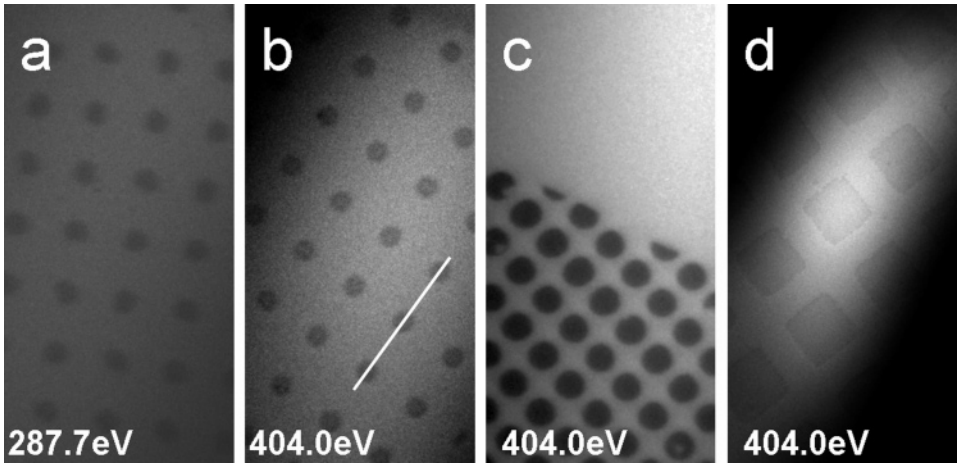

Figure 4. Raw XAM images of SAM-based lithographic patterns: (a) at the position of the R* resonance for AT/Au; (b−d) at the position of the π(N*O_2-) resonance for NBPT/Au. The photon energies for each image are labeled. The diameter of the dots in panels a and b is 1 μm; in panel c, 1.2 μm. The periodicity of the pattern in panel d is 15 μm. The quadratic arrangement of the dots is seen in panel c as the quadrate border. The restriction of the illuminated area by an aperture is seen in panel d.

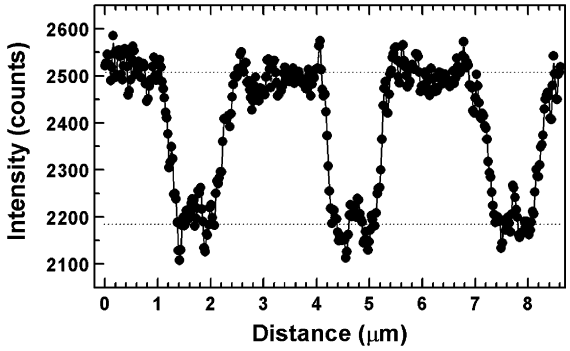

Figure 5. Intensity profile taken along the white line as indicated in Figure 4b.

patterns could be successively imaged by the latter technique, as demonstrated in Figure 4, where several raw NEXAFS images of these patterns are presented. All images show good contrast, which allows one to easily distinguish the pristine and irradiated areas, in the cases of both ≈15 μm (d) and 1−1.2 μm patterns (a−c). The interfaces between the pristine and irradiated areas are rather sharp, even for the 1−1.2 μm features (a−c). This is additionally exhibited in Figure 5, where the intensity profile along the white line as indicated in Figure 4b is given. Following this profile, 10−90% edge of the observed features (dots) could be estimated as ≈150 nm. Since this value is a convolution of the lateral resolutions for the patterning and imaging, it represents an upper limit of the XAM resolution. Considering a limited accuracy of proximity patterning, we believe that the real spatial resolution of our XAM experiment is noticeably higher.

Interestingly, the intensity profile in Figure 5 shows that the illumination of the SAMs within the dotlike openings of the membrane was inhomogeneous during the patterning: there is a systematic intensity rise in the dot centers. Considering that the initial electron flux was homogeneous, it could be only a lenslike effect of these openings, which resulted in a focusing of electrons in their centers.

The images presented in Figure 4 were acquired at photon energies corresponding to the absorption resonances. However, the contrast was observed not only at these particular adjustments but over the entire absorption edges. The reason for this was the superposition of the signals from the film and the substrate and the interplay of several different contrast mechanisms, including "pure" spectroscopic contrast (which we are interested in), topography contrast, and work function contrast. In the TEY acquisition mode, the total signal is dominated by emission from the gold substrate, whereas the intensity associated with the organic film is much lower. In particular, the most intense photoemission line of gold, Au 4f, lies at a binding energy of ≈84 eV[37,49] and contributes, along with the corresponding secondary electrons, to the total signal, even at the acquisition of the C K-edge spectrum. At higher photon energies (N and O K-edge spectra), there are additional contributions from the Au $4d_{5/2}$ (336 eV), Au $4d_{3/2}$ (354 eV), and Au $4p_{3/2}$ (547 eV) emissions.[49] Considering that the photoionization cross sections of the Au 4f, 4d, and 4p core levels are noticeably higher than those of the C 1s, N 1s, and O 1s levels (primary excitation in XAS and XAM)[50−52] and that the TEY signal from Au substrate is only weakly attenuated by the organic film,[53,54] one can assume a dominance of the substrate signal. Under these circumstances, not the differences between the NEXAFS spectra of the pristine and irradiated areas of a SAM pattern but topography and work function differences between these areas become of primary importance for the observed "total" contrast and make it almost independent of the photon energy. Both latter differences in fact exist, as suggested by the XPM experiments on AT and NBPT patterns[30,31] and by work function measurements on irradiated AT/Au and AT/Ag.[55,56]

However, whereas the contributions from the film and the substrate cannot be separated in the raw images, they can be easily distinguished in the respective microspot spectra, since the substrate-related signal is rather smooth. Raw NEXAFS microspot spectra related to the pristine and irradiated areas of the AT and NBPT patterns (1 μm dots) are presented in Figures 6 and 7, respectively. Even though the nonspecific background is rather intense in these spectra (see the intensity scale), exactly as we stated above, specific spectral features are clearly pronounced. Most important, the resonant structure and the shape of the microspot spectra for the irradiated and nonirradiated areas differ from each other (the intensity of the raw spectra for these areas cannot be directly compared due to the different illuminations of the regions selected for the integration).

The above-mentioned differences become more apparent when the normalization of the raw microspot spectra is performed (see section 2). The typical normalized NEXAFS microspot spectra of the pristine and irradiated areas of the AT and NBPT patterns (1 μm dots) are presented in Figures 8 and

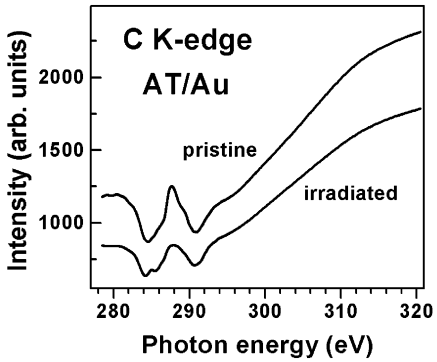

Figure 6. Raw C K-edge NEXAFS microspot spectra related to the pristine and irradiated areas of the patterned (1 μm dots) AT/Au. For a better comparison, the spectra are slightly shifted in the vertical direction with respect to each other.

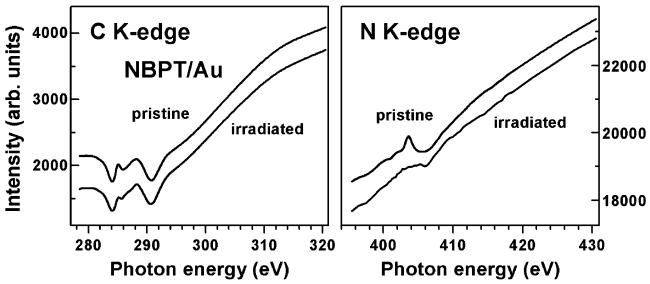

Figure 7. Raw C and N K-edge NEXAFS microspot spectra related to the pristine and irradiated areas of the patterned (1 μm dots) NBPT/Au. For a better comparison, the spectra are slightly shifted in the vertical direction with respect to each other.

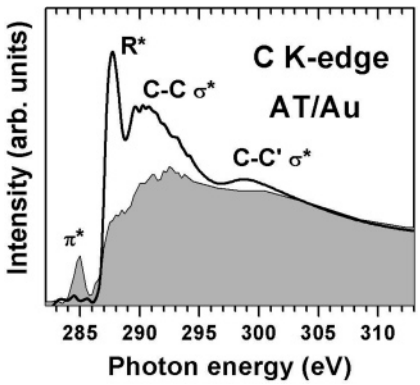

Figure 8. Normalized C K-edge NEXAFS microspot spectra related to the pristine (thick line) and irradiated (shadowed) areas of the patterned (1 μm dots) AT/Au.

9, respectively. These spectra can be directly compared with the respective spectra of the homogeneous samples in Figures 1 and 2. This comparison shows that the microspot spectra of the pristine areas exhibit all characteristic absorption resonances of the pristine films, while the microspot spectra of the irradiated areas reveal all characteristic changes upon the irradiation, just in the same way as the respective spectra of the homogeneously irradiated films. Only the weak N K-edge resonances around 400 eV are not exhibited in the case of NBPT/Au, but they are hardly perceptible even in the spectrum of the homogeneously irradiated film. Thus, the normalized NEXAFS microspot spectra are fully representative for the corresponding areas and provide specific chemical information with a high lateral resolution. An additional example of this specificity is given in Figure 10, in which the raw C K-edge NEXAFS microspectrum related to unexpected dotlike spots in the patterned NBPT/Au (one of the samples exhibited such spots) are presented along with the respective XAM image. The comparison of this microspectrum with the corresponding data in the left panels of Figure 7 suggests the appearance of an additional resonance at $\approx$297 eV, which can be associated with the π(C*═O) excitation,[33] that is, the dotlike spots represent a contamination, containing CO moieties.

4. Discussion

Within this study, we performed the characterization of the pristine and X-ray/electron-irradiated AT and NBPT SAMs and SAM-based patterns on Au substrate by several complementary spectroscopic and microscopic techniques, including NEXAFS spectroscopy, HRXPS, and XAM. The emphasis was laid on the imaging and characterization of patterned AT and NBPT films by XAM. It was found that such lithographic patterns can be easily imaged by XAM with sharp contrast and good lateral resolution, which is better than 150 nm. The observed contrast was, however, not entirely chemically specific, that is, was not exclusively governed by the specific differences in the NEXAFS spectra of the pristine and irradiated areas in the patterned SAMs. The contrast was mostly determined by the morphology and work function differences between these areas. Under optimal conditions, these differences could be of minor importance, but the emission signal for a thin organic film on a bulk metal substrate is dominated by the nonspecific substrate signal, especially in the TEY acquisition mode, which is associated with a weak attenuation of the substrate-related emission by the organic film.[53,54] The attenuation can be, however, noticeably increased, by use of the PEY or Auger electron imaging. In this case, most of the secondary electrons will be cut out and the substrate signal will consist mostly of elastic Auger electrons and photoelectrons, which undergo strong scattering in the organic film.[54] Thus, one need to introduce an energy filter into the X-PEEM to change the balance between the substrate and overlayer signals in favor of the latter emission. This experiment could not be, however, performed within the present study since our microscope is not equipped with an energy filter. Note, however, that the introduction of an energy filter into a PEEM usually reduces lateral resolution of this device, so that a compromise between the chemically specific imaging and lateral resolution should be looked for, depending on a particular goal. Note also that the contribution of the substrate will be noticeably smaller in the case of a semiconductor (e.g., Si) or oxide (e.g., SiO_2) support, since the respective electron yield is noticeably lower than that from metal substrates.[35]

It is, however, a minor problem that the images of patterned SAMs on a metal substrate are mostly not chemically specific, since even these nonspecific images clearly show the patterns. On one hand, one can apply the normalization of the images acquired at the position of the absorption resonances to the images acquired in the preedge or postedge regions. On the other hand, and this is the method of choice in our opinion, NEXAFS microspot spectra can be derived from a suitable stack of the XAM images by setting the proper areas for the integration, just in the same way as it has been done in the present study. The comparison of the presented microspot spectra for the pristine and irradiated areas of the patterned AT/Au and NBPT/Au with the analogous NEXAFS spectra acquired from the homogeneous samples suggests a comparable quality of the large-area and microspot spectra, with the same potential for the monitoring of chemical changes or differences in the samples under consideration.

Comparing the possibilities of XAM and XPM for chemical imaging and microspectroscopic characterization of monomo-

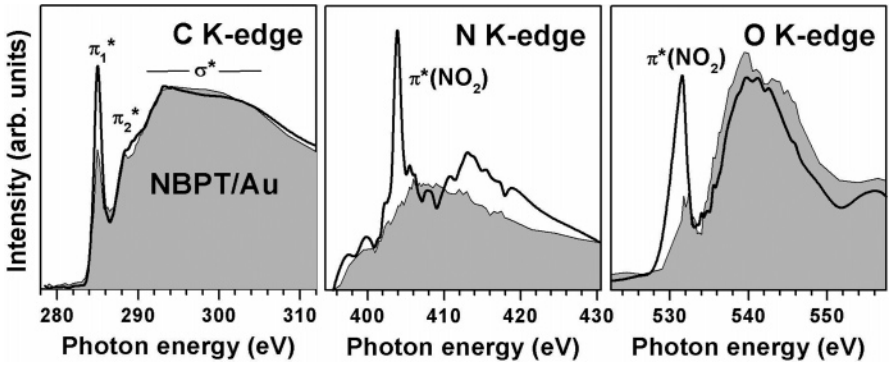

Figure 9. Normalized C, N and O K-edge NEXAFS microspot spectra related to the pristine (thick line) and irradiated (shadowed) areas of the patterned (1 μm dots) NBPT/Au.

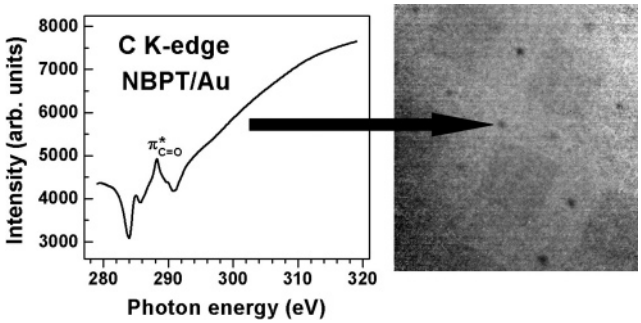

Figure 10. Raw C K-edge NEXAFS microspectrum related to dotlike spots (shown by arrow) in the patterned NBPT/Au, along with the respective XAM image.

lecular lithographic patterns, one can say that both techniques have definite advantages and disadvantages. XPM is capable of chemical imaging, at least at the adjustment of the microscope to intense emissions.[15,30,31] The imaging at the position of weak emissions, such as, for example, the peaks associated with nitro and amino groups in the pristine and modified NBPT films (see Figure 3), is, however, not possible so far due to a strong inelastic background, which smears the specific contrast associated with the elastic signal.[31] An additional problem is the damage caused by the focused X-ray beam during the image acquisition, which limits the dwell time for the imaging, making the acquisition of image stacks hardly possible. The latter constraint makes it difficult to obtain XPM microspot spectra from patterned SAMs over an extended range of binding energies. Note, however, that rough, short-range XPM microspot spectra can be acquired if multichannel detection of the emission signal is used.[31] Note also that one can turn the disadvantage into an advantage and use the impact of the focused X-ray beam for direct patterning of monomolecular resist.[15]

In contrast to XPM, XAM does not provide direct chemical imaging of the SAM patterns on metal substrates, at least in the TEY acquisition mode. This technique is, however, capable of nonspecific imaging of the respective patterns, with subsequent laterally resolved chemical information provided by the NEXAFS microspot spectra taken from any areas of interest. The X-ray damage seems to be a lesser problem in the case of XAS as compared to XPM: no changes in the NEXAFS spectra were observed after the acquisition of the image stack at a selected absorption edge, as long as reasonable precautions were taken (see section 2). Such a stack allowed us to derive the microspot spectra for all relevant areas of interest within the field of view. This procedure helps to avoid the problem of intense nonspecific background, since the characteristic absorption features are clearly exhibited in the microspot spectra. In particular, a chemical transformation of the functional tail groups within the irradiated areas of the patterned aromatic SAMs could be directly monitored, which was not possible so far in the case of XPM. Finally, the current lateral resolution of XAM ($<$150 nm) is noticeably better than that of XPM ($\approx$500 nm). These values depend, however, on the specific experimental setup and can be improved in the case of both XPM and XAM.

The presented XAM results suggest that the conclusions derived on the basis of the spectroscopic data for the homogeneously irradiated SAM systems are generally applicable to SAM-based lithographic patterns—the same chemical and physical changes occur in a homogeneously irradiated SAM and within a small irradiated spot. At the same time, the XAM data show that there can be inhomogeneities within these spots, which stem from a specific way of SAM pattern fabrication. In the case of proximity patterning, used in this study, this was a focusing of the electron beam by the openings in the conductive mesh, which was responsible for the inhomogeneous exposure of the irradiated spots. In the case of direct patterning by a focused electron or X-ray beam, these can the effects of the beam profile. Also, the inhomogeneity of the SAM itself can affect the quality of the fabricated pattern, if a high-resolution patterning is performed.[10]

5. Summary

X-ray absorption microscopy was applied for the imaging and characterization of lithographic patterns fabricated by electron irradiation of AT and NBPT SAMs on Au. The patterns could be clearly imaged by XAM. The observed contrast resulted from an interplay of chemically specific spectromicroscopic contrast and nonspecific topographic and work function contrasts. The lateral resolution was estimated to be better than 150 nm, which, for example, allowed us to distinguish fine structure of 1 μm features. The microspot spectra derived from different areas of the SAM patterns provide specific chemical information. Even at a feature size of 1 μm, the quality of the microspot spectra was comparable with that of the analogous NEXAFS spectra acquired from homogeneous SAM samples.

There is a noticeable potential for the achievement of "truly" chemical imaging, optimization of the experimental parameters, and improvement of the lateral resolution within the XAM approach. The presented results, and in particular direct comparison of the NEXAFS and microspot spectra, clearly demonstrate that this technique can be successfully applied to the microspectroscopic characterization of even such delicate (irradiation sensitivity) and unfavorable (huge nonspecific background) objects as patterned monomolecular films on metal substrates.

Acknowledgment. We thank M. Grunze (Universität Heidelberg) for the support of this work, Ch. Wöll (Universität Bochum) for providing us with the experimental equipment for the measurements at BESSY II, L. S. O. Johansson (Karlstad University) for the cooperation at MAX-lab, W. Eck (Universität Heidelberg) for the synthesis of NBPT, and the ALS, BESSY II, and MAX-lab staff, and in particular A. Doran (ALS), for their assistance during the experiments. This work has been supported by the German BMBF (GRE1HD and 05KS4VHA/4), the Fonds der Chemischen Industrie, and by the Director, Office of Science, Office of Basic Energy Sciences, of the U.S. Department of Energy under Contract DE-AC03-76SF00098.

References and Notes

(1) Tiberio, R. C.; Craighead, H. G.; Lercel, M. J.; Lau, T.; Sheen, C. W.; Allara, D. L. *Appl. Phys. Lett.* **1993**, *62*, 476.

(2) Lercel, M. J.; Tiberio, R. C.; Chapman, P. F.; Craighead, H. G.; Sheen, C. W.; Parikh, A. N.; Allara, D. L. *J. Vac. Sci. Technol. B* **1993**, *11*, 2823.

(3) Calvert, J. M.; Koloski, T. S.; Dressick, W. J.; Dulcey, C. S.; Peckerar, M. C.; Cerrina, F.; Taylor, J. W.; Suh, D.; Wood, O. R., II; MacDowell, A. A.; D'Souza, R. *Opt. Ing.* **1993**, *32*, 2437.

(4) Lercel, M. J.; Redinbo, G. F.; Pardo, F. D.; Rooks, M.; Tiberio, R. C.; Simpson, P.; Craighead, H. G.; Sheen, C. W.; Parikh, A. N.; Allara, D. L. *J. Vac. Sci. Technol. B* **1994**, *12*, 3663.

(5) Lercel, M. J.; Rooks, M.; Tiberio, R. C.; Craighead, H. G.; Sheen, C. W.; Parikh, A. N.; Allara, D. L. *J. Vac. Sci. Technol. B* **1995**, *13*, 1139.

(6) Müller, H. U.; David, C.; Völkel, B.; Grunze, M. *J. Vac. Sci. Technol. B* **1995**, *13*, 2846.

(7) David, C.; Müller, H. U.; Völkel, B.; Grunze, M. *Microelectron. Eng.* **1996**, *30*, 57.

(8) Lercel, M. J.; Craighead, H. G.; Parikh, A. N.; Seshadri, K.; Allara, D. L. *Appl. Phys. Lett.* **1996**, *68*, 1504.

(9) Hild, R.; David, C.; Müller, H. U.; Völkel, B.; Kayser, D. R.; Grunze, M. *Langmuir* **1998**, *14*, 342.

(10) Gölzhäuser, A.; Geyer, W.; Stadler, V.; Eck, W.; Grunze, M.; Edinger, K.; Weimann, Th.; Hinze, P. *J. Vac. Sci. Technol. B* **2000**, *18*, 3414.

(11) Yang, X. M.; Peters, R. D.; Kim, T. K.; Nealey, P. F.; Brandow, S. L.; Chen, M.-S.; Shirey, L.-M.; Dressick, W. J. *Langmuir* **2001**, *17*, 228.

(12) Zharnikov, M.; Grunze, M. *J. Vac. Sci. Technol. B* **2002**, *20*, 1793.

(13) Kim, S. O.; Solak, H. H.; Stoykovich, M. P.; Ferrier, N. J.; de Pablo, J. J.; Nealey, P. F. *Nature* **2003**, *424*, 411.

(14) La, Y.-H.; Jung, Y. J.; Kim, H. J.; Kang, T.-H.; Ihm, K.; Kim, K.-J.; Kim, B.; Park, J. W. *Langmuir* **2003**, *19*, 4390.

(15) Klauser, R.; Huang, M.-L.; Wang, S.-C.; Chen, C.-H.; Chuang, T. J.; Terfort, A.; Zharnikov, M. *Langmuir* **2004**, *20*, 2050.

(16) (a) Ulman, A. *An Introduction to Ultrathin Organic Films: Langmuir−Blodgett to Self-Assembly*; Academic Press: New York, 1991. (b) Ulman, A. *Chem. Rev.* **1996**, *96*, 1533.

(17) Schreiber, F. *Prog. Surf. Sci.* **2000**, *65*, 151.

(18) Küller, A.; Eck, W.; Stadler, V.; Geyer, W.; Gölzhäuser, A. *Appl. Phys. Lett.* **2003**, *82*, 3776.

(19) Wirde, M.; Gelius, U.; Dunbar, T.; Allara, D. L. *Nucl. Instrum. Methods Phys. Res., Sect. B* **1997**, *131*, 245.

(20) Jäger, B.; Schürmann, H.; Müller, H. U.; Himmel, H.-J.; Neumann, M.; Grunze, M.; Wöll, Ch. *Z. Phys. Chem.* **1997**, *202*, 263.

(21) Müller, H. U.; Zharnikov, M.; Völkel, B.; Schertel, A.; Harder, P.; Grunze, M. *J. Phys. Chem. B* **1998**, *102*, 7949.

(22) Zharnikov, M.; Geyer, W.; Gölzhäuser, A.; Frey, S.; Grunze, M. *Phys. Chem. Chem. Phys.* **1999**, *1*, 3163.

(23) Zharnikov, M.; Frey, S.; Heister, K.; Grunze, M. *Langmuir* **2000**, *16*, 2697.

(24) Heister, K.; Zharnikov, M.; Grunze, M.; Johansson, L. S. O.; Ulman, A. *Langmuir* **2001**, *17*, 8.

(25) Geyer, W.; Stadler, V.; Eck, W.; Zharnikov, M.; Gölzhäuser, A.; Grunze, M. *Appl. Phys. Lett.* **1999**, *75*, 2401.

(26) Eck, W.; Stadler, V.; Geyer, W.; Zharnikov, M.; Gölzhäuser, A.; Grunze, M. *Adv. Mater.* **2000**, *12*, 805.

(27) Frey, S.; Rong, H.-T.; Heister, K.; Buck, M.; Zharnikov, M. *Langmuir* **2002**, *18*, 3142.

(28) Moon, J. H.; Kim, K.-J.; Kang, T.-H.; Kim, B.; Kang, H.; Park, J. W. *Langmuir* **1998**, *14*, 5673.

(29) Gölzhäuser, A.; Eck, W.; Geyer, W.; Stadler, V.; Weimann, T.; Hinze, P.; Grunze, M. *Adv. Mater.* **2001**, *13*, 806.

(30) Klauser, R.; Hong, I.-H.; Lee, T.-H.; Yin, G.-C.; Wei, D.-H.; Tsang, K.-L.; Chuang, T. J.; Wang, S.-C.; Gwo, S.; Zharnikov, M.; Liao, J.-D. *Surf. Rev. Lett.* **2002**, *9*, 213.

(31) Klauser, R.; Hong, I.-H.; Wang, S.-C.; Zharnikov, M.; Paul, A.; Gölzhäuser, A.; Terfort, A.; Chuang, T. J. *J. Phys. Chem. B* **2003**, *107*, 13133.

(32) Köhn, F. Diploma Thesis, Universität Heidelberg, Heidelberg, Germany, 1998.

(33) Stöhr, J. *NEXAFS Spectroscopy*; Springer Series in Surface Science 25; Springer-Verlag: Berlin, 1992.

(34) Batson, P. E. *Phys. Rev. B* **1993**, *48*, 2608.

(35) Laibinis, P. E.; Graham, R. L.; Biebuyck, H. A.; Whitesides, G. M. *Science* **1991**, *254*, 981.

(36) Heister, K.; Zharnikov, M.; Grunze, M.; Johansson, L. S. O. *J. Phys. Chem. B* **2001**, *105*, 4058.

(37) *Surface chemical analysis−X-ray photoelectron spectrometers−Calibration of the energy scales*; ISO 15472, 2001.

(38) Outka, D. A.; Stöhr, J.; Rabe, J. P.; Swalen, J. D. *J. Chem. Phys.* **1988**, *88*, 4076.

(39) Hähner, G.; Kinzler, M.; Thümmler, C.; Wöll, Ch.; Grunze, M. *J. Vac. Sci. Technol.* **1992**, *10*, 2758.

(40) Bagus, P. S.; Weiss, K.; Schertel, A.; Wöll, Ch.; Braun, W.; Hellwig, H.; Jung, C. *Chem. Phys. Lett.* **1996**, *248*, 129.

(41) Väterlein, P.; Fink, R.; Umbach, E.; Wurth, W. *J. Phys. Chem.* **1998**, *108*, 3313.

(42) Zharnikov, M.; Grunze, M. *J. Phys.: Condens. Matter* **2001**, *13*, 11333.

(43) Giebler, R.; Schulz, B.; Reiche, J.; Brehmer, L.; Whn, M.; Wll, Ch.; Smith, A. P.; Urquhart, S. G.; Ade, H. W.; Unger, W. E. S. *Langmuir* **1999**, *15*, 1291.

(44) Zubavichus, Y.; Zharnikov, M.; Shaporenko, A.; Grunze, M.; Fuchs, O.; Weinhardt, L.; Heske, C.; Umbach, E.; Denlinger, J. D. *J. Phys. Chem. A* **2004**, *108*, 4557.

(45) Gordon, M. L.; Cooper, G.; Morin, C.; Araki, T.; Turci, C. C.; Kaznatcheev, K.; Hitchcock, A. P. *J. Phys. Chem. A* **2003**, *107*, 6144.

(46) Zubavichus, Y.; Zharnikov, M.; Shaporenko, A.; Grunze, M. *J. Electron Spectrosc. Relat. Phenom.* **2004**, *134*, 25.

(47) Bierbaum, K.; Kinzler, M.; Wll, Ch.; Grunze, M.; Hhner, G.; Heid, S.; Effenberger, F. *Langmuir* **1995**, *11*, 512.

(48) Shaporenko, A.; Harder, P.; Allara, D. L.; Zharnikov, M. To be published.

(49) Moulder, J. F.; Stickle, W. E.; Sobol, P. E.; Bomben, K. D. *Handbook of X-ray Photoelectron Spectroscopy*; Chastian, J., Ed.; Perkin-Elmer Corp.: Eden Prairie, MN, 1992.

(50) Band, I. M.; Kharitonov, Yu. I.; Trzhaskovskaya, M. B. *At. Data Nucl. Data Tables* **1979**, *23*, 443.

(51) Goldberg, S. M.; Fadley, C. S.; Kono, S. *J. Electron Spectrosc. Relat. Phenom.* **1981**, *21*, 285.

(52) Yeh, J. J.; Lindau, I. *At. Data Nucl. Data Tables* **1985**, *32*, 1.

(53) Ohara, H.; Yamamoto, Y.; Kajikawa, K.; Ishii, H.; Seki, K.; Ouchi, Y. *J. Synchrotron Radiat.* **1999**, *6*, 803.

(54) Zharnikov, M.; Frey, S.; Heister, K.; Grunze, M. *J. Electron. Spectrosc. Relat. Phenom.* **2002**, *124*, 15.

(55) Chenakin, S. P.; Heinz, B.; Morgner, H. *Surf. Sci.* **1998**, *397*, 84.

(56) Chenakin, S. P.; Heinz, B.; Morgner, H. *Surf. Sci.* **1999**, *421*, 337.